

Mechanical Properties and Fracture Behaviors of GTA-Additive Manufactured 2219-Al After an Especial Heat Treatment

J.Y. Bai, C.L. Fan, S.B. Lin, C.L. Yang, and B.L. Dong

(Submitted July 22, 2016; in revised form February 15, 2017; published online March 21, 2017)

2219-Al parts were produced by gas tungsten arc-additive manufacturing and sequentially processed by an especial heat treatment. In order to investigate the effects of heat treatment on its mechanical properties, multiple tests were conducted. Hardness tests were carried out on part scale and layer scale along with tensile tests which were performed on welding and building directions. Results show that compared to conventional casting + T6 2219-Al, the current deposit + T6 2219-Al exhibits satisfying properties with regard to strength but unsatisfying results in plasticity. Additionally, anisotropy is significant. Fractures were observed and the cracks' propagating paths in both directional specimens are described. The effects of heat treatment on the cracks' initiation and propagation were also investigated. Ultimately, a revised formula was developed to calculate the strength of the deposit + T6 2219-Al. The aforementioned formula, which takes into consideration the belt-like porosities-distributing feature, can scientifically describe the anisotropic properties in the material.

Keywords additive manufacturing, aluminum, fracture behaviors, GTA, mechanical properties

1. Introduction

GTA-additive manufacturing, which uses the heat of GTAW (gas tungsten arc welding) to melt materials, is a low-cost and highly efficient technique to produce near-net structures directly from CAD files (Ref 1-6). So far, many materials can be produced using this technique, of which Ti alloys (Ref 7) and Ni alloys (Ref 8) are the most popular. Due to the low strength, little research has been conducted on Al alloys. However, some high-strength Al alloys are widely used in aviation and aerospace fields, such as the 2xxx, 6xxx and 7xxx series. Thus, it is necessary to give more attention to them. Since 6xxx welding wire and 7xxx welding wire are so far not available, current research is conducted on the 2xxx Al alloy (2219-Al).

In earlier research of 2219-Al, Bai and Wang (Ref 9-11) found that the tensile strength of the as-deposited 2219-Al (GTA-additive manufactured 2219-Al) is only equal to 58% of the conventional casting + T6 2219-Al (under routinely used conditions). Because 2219-Al is a typical precipitation-strengthening material, heat treatment is an appropriate choice to improve the strength. However, due to the unconventional manufacturing method, the conventional heat treatment is ineffective in as-deposited materials. Fortunately, much research has been conducted on different materials. In 2012, an

exceptional solution + aging technique was proposed by Erhard (Ref 12, 13). After heat treatment, an isotropic mechanical property was obtained for TC4. In 2015, a homogenization technique was developed by Yadollahi for 318L steel (Ref 14). Though elongation was improved, it was achieved at the expense of strength. In 2013, three techniques were conducted for Inconel 625 by Xu (Ref 15). Finally, the solution heat treatment was regarded as the best method. After heat treatment, the segregation of the Nb element was eliminated. In 2013, a solution heat treatment was carried out on 5356-Al by Jiang (Ref 16), but the effects turned out to be anisotropic. In building direction, both strength and elongation were improved. However, in welding direction, the strength and elongation were reduced.

The mechanical properties after heat treatment are still not known. The appropriate technique for as-deposited high-strength Al alloy (2219-Al) is also an unknown along with whether anisotropy will occur. Nearly everything is unknown in this new field. In the current study, an especial homogenized solution + aging technique is proposed for 2219-Al. The mechanical properties and fracture behaviors are the main focus of the presented research.

2. Experiments

A GTA-additive manufacturing process was carried out on a modified GTA-welding system, by which thin-walled (multi-layers and single-pass) plate and cylinders were produced (Fig. 1). The thin-walled plate was selected for tests. In building direction, the plate is 100 layers in height. And in welding direction, it is 20 mm in length. The welding parameters in each layer are identical: The welding current is 103 A; the welding speed is 200 mm/min; the wire feeding rate is 1000 mm/min; and the resident temperature is 80 ± 10 °C.

As shown in Fig. 2, in the manufacturing process of conventional casting + T6 2219-Al, a homogenization treatment

J.Y. Bai, C.L. Fan, S.B. Lin, C.L. Yang, and B.L. Dong, State Key Laboratory of Advanced Welding and Joining, Harbin Institute of Technology, No. 92 West-Dazhi Street, Harbin 150001, China. Contact e-mails: baijiuyang-123@163.com and sblin@hit.edu.cn.

and a solution treatment are carried out separately before and after the rolling process. In this paper, the homogenization treatment and solution treatment are combined; thus, a homogenized solution treatment is proposed. Compared to the conventional solution treatment (whose holding time is about 30 min), the current homogenized solution treatment is characterized by an exceptionally long holding time.

In the selection of the parameters for the homogenized solution treatment, different holding temperatures and holding times were tested. Ultimately, 530 °C and 20 h were decided for the holding temperature and the holding time. Aging parameters were obtained from the handbook (Ref 17), from which the holding temperature was 175 °C and the holding time was 17 h.

After heat treatment, hardness tests were conducted on the deposit-T6 2219-Al parts. Since the 2219-Al exhibits a layered-division feature (Ref 9), 0.5-mm (part scale) and 0.1-mm (layer scale) intervals were adopted between measuring points. The tests were carried out on THV-5, in which the loading was 200 g. Since anisotropy is common in additive manufactured materials, tensile tests were performed in welding and building directions of the plate (Fig. 3). The tensile specimens were first processed with wire electrodes cut to 2.0 mm and sequentially polished by abrasive paper. Fractures and microstructures were observed through SEM (scanning electron microscope), TEM (transmission electron microscope) and OM (optical microscope).

3. Mechanical Properties

3.1 Microstructures

In order to better understand the mechanical properties, the microstructures of deposit + T6 2219-Al are shown in Fig. 4.



Fig. 1 GTA-additive manufactured 2219-Al parts

Because of the layer-adding manufacturing method, the microstructures present a layered-division feature. In the inner-layer regions, fine and discontinuous eutectic structures (θ -Al₂Cu + α -Al) dominate. While in interface regions, there are many bulk-like eutectic structures.

Because the solubility of the hydrogen element in liquid Al alloy is about 20 times greater than in solid Al alloy, a significant amount of the hydrogen element separates out during solidification. Additionally, the interface is at the bottom of the molten pool where the solidification rate is the fastest. Hydrogen porosities are easily formed there and have no time to escape. Eventually, porosities distribute along the interface and exhibit a belt-like feature. After heat treatment, porosities were still located at the bottom.

Though many methods can control porosity, such as reducing heat input and by increasing the welding speed and layer height, they cannot be completely avoided. As a result, though the GTA-additive manufacturing parameters are optimized, porosity still exists. Usually, the size of the porosities is smaller than 80 μ m. Since they cannot be observed directly by the naked eye, they are generally classified as microporosities. Because of their belt-like distribution, the porosities would potentially cause damage to the material and more attention needs to be given to them in the future studies.

3.2 Hardness

Hardness is an important factor in evaluating the mechanical properties, and the distribution of it can describe the uniformity of the material. Figure 5 plots the hardness in relation to the distance for the part scale, and the interval is 0.5 mm. Results show that the material presents a uniform hardness along the building direction. It means that height does not have an effect on the mechanical properties. The average hardness is 148.8 HV_{0.2}, exceeding the value of as-deposited 2219-Al by more than 90%. Moreover, compared to a conventional casting + T6 2219-Al (144.5 HV_{0.2}), the current deposit + T6 2219-Al also exhibits a better property.

Since the deposited 2219-Al exhibits a layered-division feature, the influence of interfaces and inner-layers on hardness needs further investigation. Thus, 0.1-mm intervals are adopted for the layer scale in region B (Fig. 6). Centering on one of the layers, hardness distributions are shown in Fig. 6. Since the process of GTA-additive manufacturing could be regarded as a special type of GTA-welding, the deposited layers could be equivalent to welding beads. Thus, the interfaces are equivalent to fusion zones in the GTA-welding. Usually, in 2219-Al GTA-welding the hardness presents a “w” distribution centering on the welding bead, of which the fusion zones have the bottom value (Ref 18). However, this typical feature is absent in not only as-deposited 2219-Al (Ref 10) but also the deposit + T6

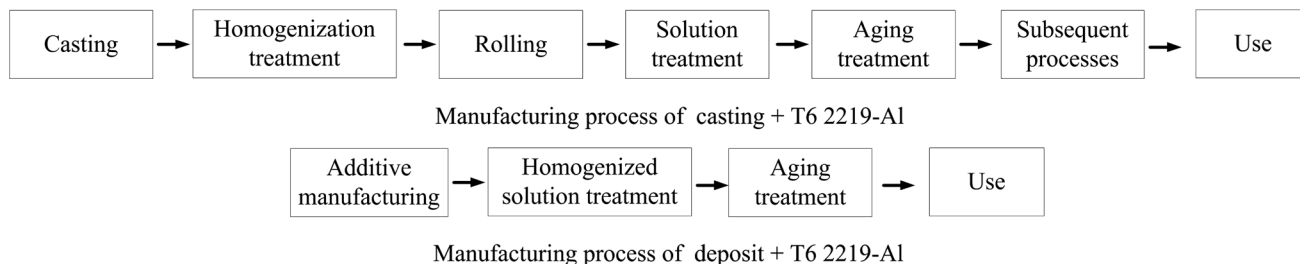


Fig. 2 Manufacturing process of conventional casting-T6 and deposit-T6 2219-Al parts

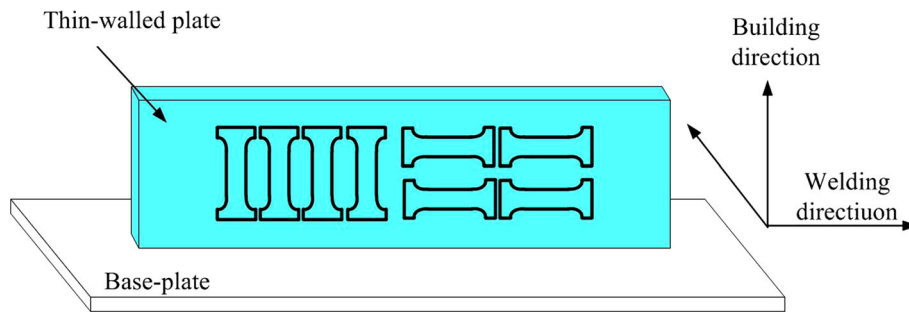


Fig. 3 Directions definition and tensile specimens extraction in thin-walled plate

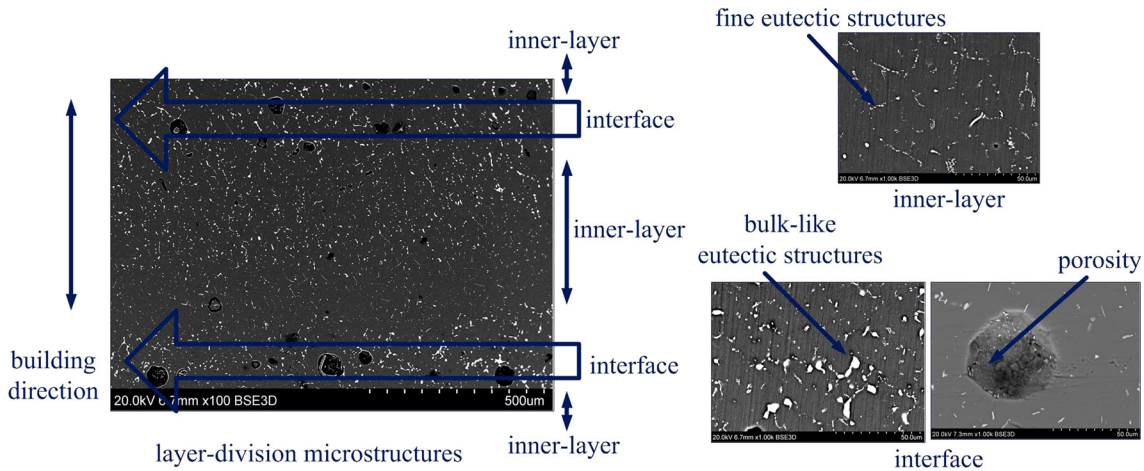


Fig. 4 Microstructures of deposit + T6 2219-Al

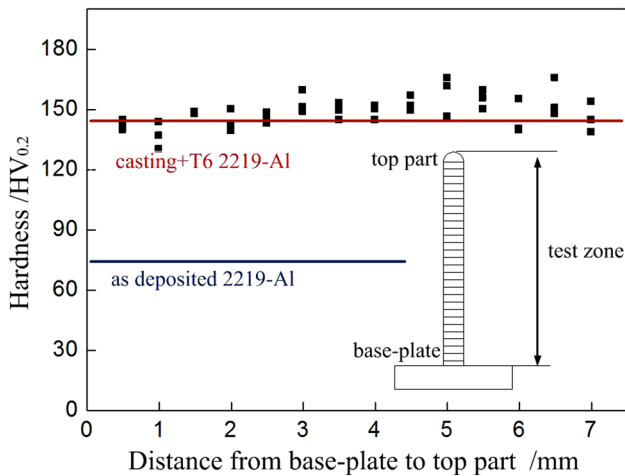


Fig. 5 Hardness distribution on part scale

2219-Al (Fig. 5). The hardness presents uniform values in interfaces and inner-layers.

3.3 Tensile Properties

In tensile tests, 32 specimens are included, of which 16 specimens are extracted from the welding direction and the other specimens are extracted from the building direction. The average yield strength, ultimate strength and elongation of deposit + T6 2219-Al are 266 ± 22 , 391 ± 28 MPa and 8.3%,

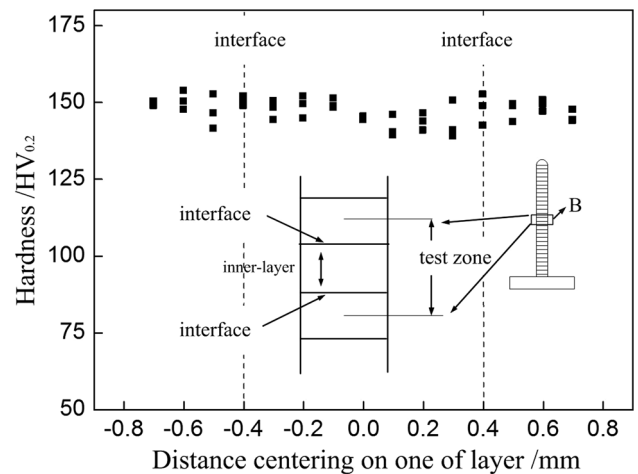


Fig. 6 Hardness distribution in region B (on layer scale)

respectively. In Fig. 7, to evaluate the effects of heat treatment, properties of conventional casting + T6 2219-Al and as-deposited 2219-Al are also signified. After the heat treatment, the ultimate strength is improved by 65%, but the elongation is reduced by 17%. Compared to the properties of casting + T6 2219-Al, the deposit + T6 2219-Al has satisfactory properties in strength but unsatisfactory results in plasticity. The yield strength and ultimate strength are 91.7 and 94.3% of the properties of conventional casting + T6 2219-Al, whereas the elongation is only as little as 55.3%.

Taking the welding and building directions into consideration, the anisotropic mechanical properties are also significant in deposit + T6 2219-Al (Fig. 8). The yield strength, ultimate strength and elongation are 269 ± 28 , 418 ± 22 MPa and 10.24%, respectively, in the welding direction, whereas the values are 254 ± 28 , 365 ± 28 MPa and 7.44% in the building

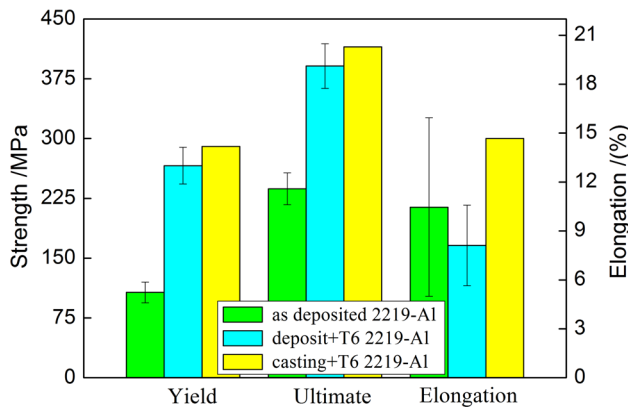


Fig. 7 Tensile results

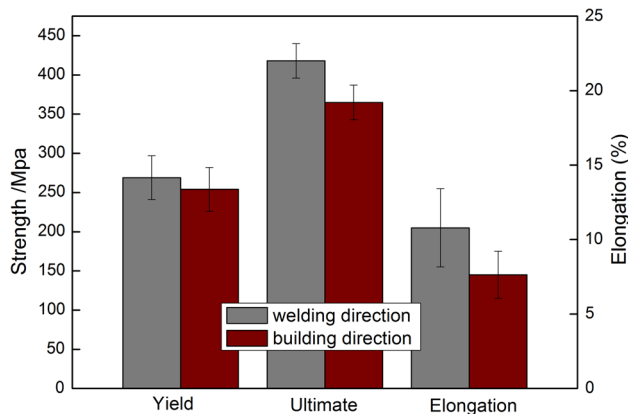


Fig. 8 Anisotropy in tensile properties

direction. These gaps are so remarkable between the two directions that they cannot be simply regarded as experimental or statistical errors.

In summary, the tensile properties are higher in the welding direction than in the building direction. Additionally, it should be noted that the properties in welding direction are very inspiring. The yield strength and ultimate strength can be as much as 92.7 and 100.8% of the properties of casting + T6 2219-Al. Under the current situation, the early application of 2219-Al may be applied in welding direction.

3.4 Fracture Behaviors

3.4.1 Side-Faces Observation. In the welding direction specimen, the tensile direction and building direction are vertical (Fig. 9a). The fracture propagates vertically across the interfaces, and no tearing phenomenon occurs between layers. While in the building direction specimen, building and tensile directions are consistent. Fractures propagate along one of the interfaces (Fig. 9b). Since eutectic structures and porosities are typical ingredients in interfaces, they will be focused upon the future studies.

In as-deposited 2219-Al, many eutectic structures are continually distributed (Fig. 10a and b). Because the eutectic structures have low plasticity properties, they are the weak points of the material. As shown in Fig. 10(a), in a tensile test, the eutectic structures in and near to porosity areas are ruptured into pieces, but the porosity itself is intact. That means the eutectic structures rupture before the porosity and they are more likely to be the initiation of a crack. Moreover, as shown in Fig. 10(b), there are many rupturing eutectic structures remaining along the boundaries of the fracture. That means the cracks are more likely to propagate along the distributing path of the eutectic structures. All the evidence suggests that the eutectic structure characteristics are more detrimental than the porosities in as-deposited 2219-Al (Ref 10).

However, in deposit + T6 2219-Al, most of the eutectic structures are dissolved after heat treatment (Fig. 4), and the eutectic structures are no longer the main causes of cracks' initiation and propagation. Therefore, other ingredients need to be investigated. Figure 10(c) describes that the porosities contribute to the initiation of cracks in deposit + T6 2219-Al.

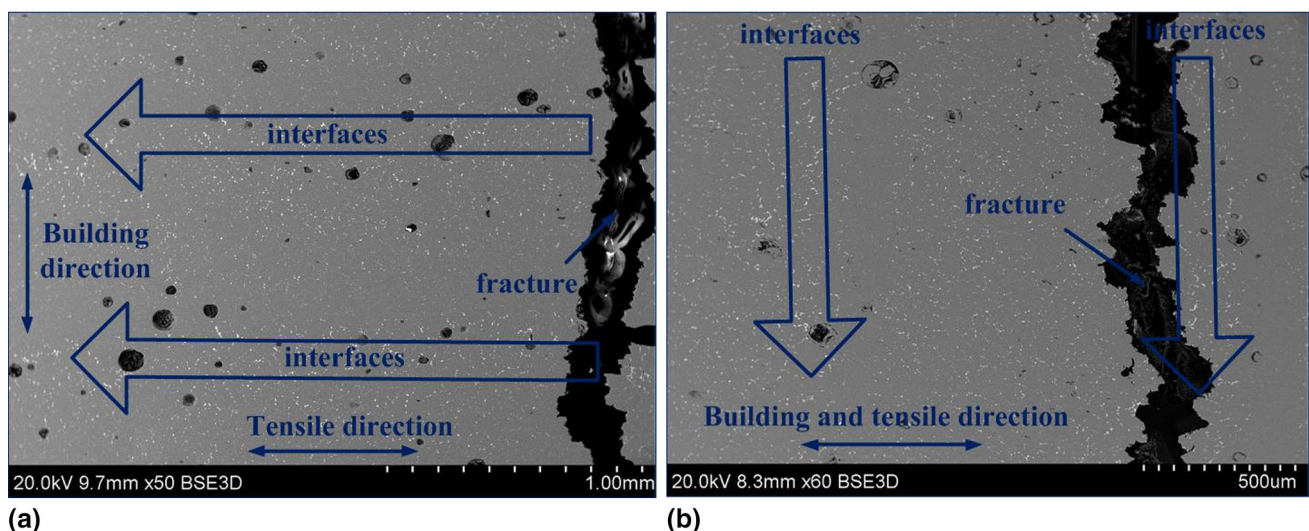


Fig. 9 Fracture propagating paths in (a) welding directional specimen and (b) building directional specimen

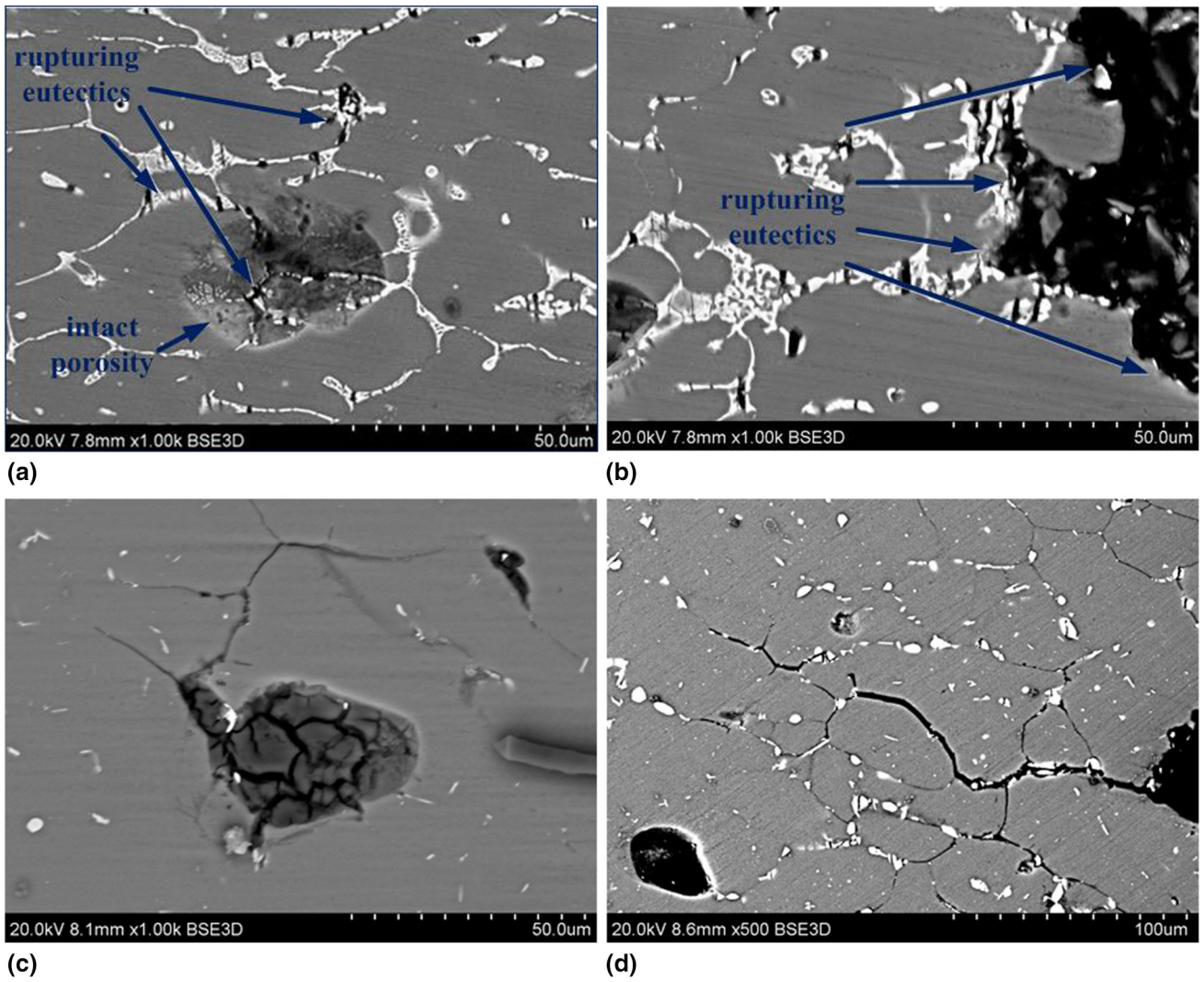


Fig. 10 Side-face observation (a) initiation of a crack in as-deposited 2219-Al, (b) crack propagating path in as-deposited 2219-Al, (c) initiation of a crack in deposit + T6 2219-Al and (d) crack propagating path in deposit + T6 2219-Al

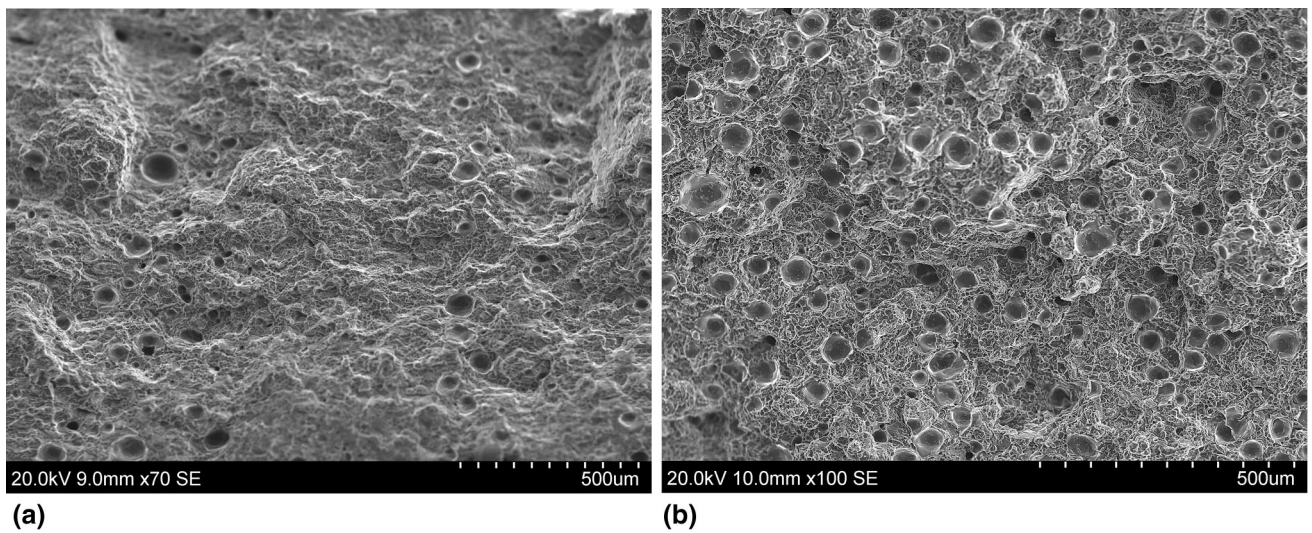


Fig. 11 Front-face of fractures in (a) welding direction specimen and (b) building direction specimen

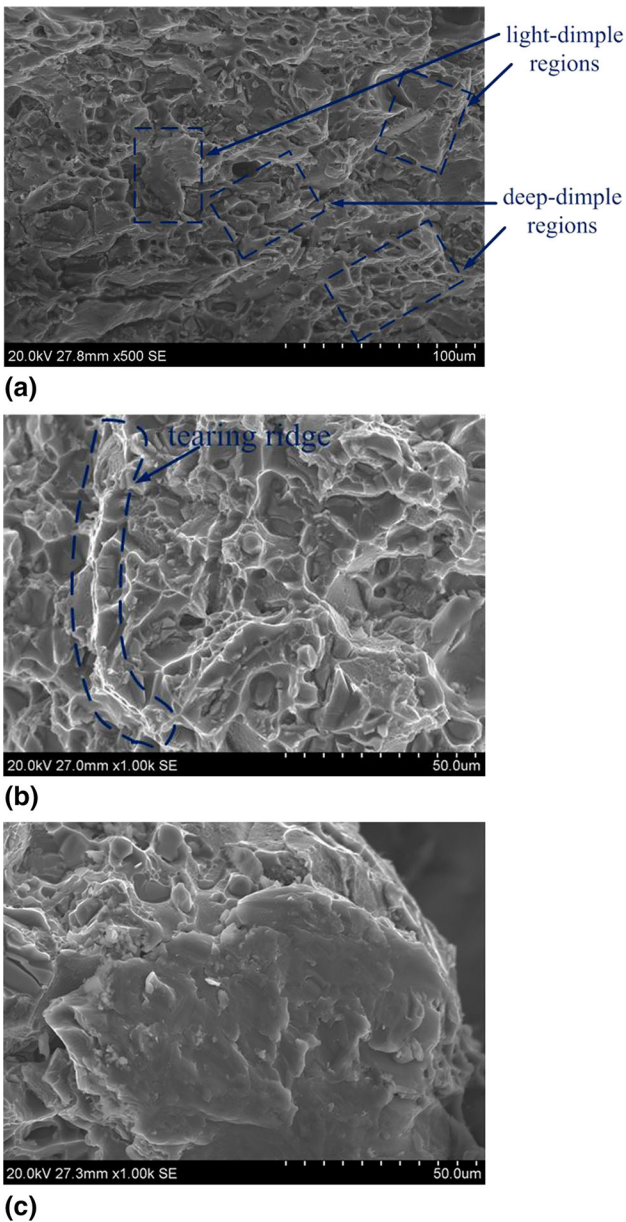


Fig. 12 Details of the fracture (a) dimples in fractures, (b) deep-dimple region and (c) light-dimple region

Because of the stress concentration, the cracks are more likely to be initiated at the dendrite clearances near to and inside the porosity. Additionally, the cracks exhibit an equiaxed propagating path along the boundaries of the equiaxed grains (Fig. 10d). The equiaxed propagating path suggests that the grain boundaries are also the potential weak points.

3.4.2 Front-Faces Observation. Figure 11(a) and (b) shows front-face of fractures in welding and building direction specimens. The surfaces are coarse in both fractures. Particularly, there are a lot of porosities distributed in the fractures. However, the distributing types are quite different in the two directional fractures. In the welding direction fracture, porosities present a belt-like distribution and two belts can be discerned. However, in the building direction fracture, porosities are homogeneously distributed.

As mentioned before, porosities are more likely to occur at the interfaces. In the welding direction specimen, tensile forces

are loaded parallel to the interfaces and consequently, fractures propagate across them (Fig. 9a). While in the building direction specimen, tensile forces and interfaces are perpendicular causing fractures to propagate along the entire interface (Fig. 9b). As a result, the two interface side-views are presented in a welding direction fracture (Fig. 11a), while an entire interface front-view is shown in the building direction fracture (Fig. 11b).

In addition to the porosities, there are many dimples in the fractures of both directions. Generally speaking, dimples are the typical features of a ductile fracture. However, the dimples do not occur uniformly (Fig. 12a). The deep-dimple regions and the light-dimple regions are distributed simultaneously. The dimples in the deep-dimple regions are much deeper (Fig. 12b). While in the light-dimple regions, the surface is planar and only some tiny dimples occur (Fig. 12c). The presentation of light-dimple regions describes the low plasticity property in deposit + T6 2219 Al.

4. Discussion

4.1 Mechanism of Strengthening

Generally speaking, the strength of 2xxx (σ_{2xxx}) Al alloy can be obtained in the following areas: strength of the Al matrix (σ_{base}), grain boundary strengthening (σ_{gbs}), solution strengthening (σ_{ss}), dislocations strengthening (σ_{ds}), and precipitation strengthening (σ_{ps}).

$$\sigma_{2xxx} = \sigma_{base} + \sigma_{gbs} + \sigma_{ss} + \sigma_{ds} + \sigma_{ps} \quad (\text{Eq 1})$$

However, no rolling or deforming process occurs during both the GTA-additive manufacturing and the heat treatment process (Fig. 2), meaning that σ_{ds} is absent. Therefore, the strength of the GTA-additive manufactured 2xxx Al alloy (σ_{AM}) can be expressed as Eq 2:

$$\sigma_{AM} = \sigma_{base} + \sigma_{gbs} + \sigma_{ss} + \sigma_{ps} \quad (\text{Eq 2})$$

Before the heat treatment, the value of σ_{ps} is negligible in as-deposited 2219-Al (Ref 11). However, precipitation strengthening (σ_{ps}) is a vital part of σ_{AM} . Therefore, compared to conventional casting + T6 2219-Al, the value of the as-deposited 2xxx Al alloy ($\sigma_{deposit}$) is much lower.

$$\sigma_{deposit} = \sigma_{base} + \sigma_{gbs} + \sigma_{ss} \quad (\text{Eq 3})$$

After the homogenized solution heat treatment, the values of σ_{base} and σ_{gbs} are invariable. However, σ_{ss} can be improved to a peak value.

For the aging process, many θ' -Al₂Cu phases precipitate at the expense of some Cu-solutes. Though σ_{ss} decreases, σ_{ps} increases to a large degree. It can be considered that, in deposit + T6 2219-Al, most of the strengthening effects are obtained from the increase in σ_{ps} .

$$\sigma_{deposit+T6} = \sigma_{base} + \sigma_{gbs} + \sigma_{ss} + \sigma_{ps} \quad (\text{Eq 4})$$

Though the precipitation of the θ' phases increases the strength properties, it is achieved at the expense of plasticity. The precipitation of the θ' phases inhibits the dislocations' gliding in a tensile test. As a result, the elongation decreases 17% after the heat treatment.

For the current situation, the low plasticity compared to conventional casting + T6 2219-Al can be ascribed to the coarse

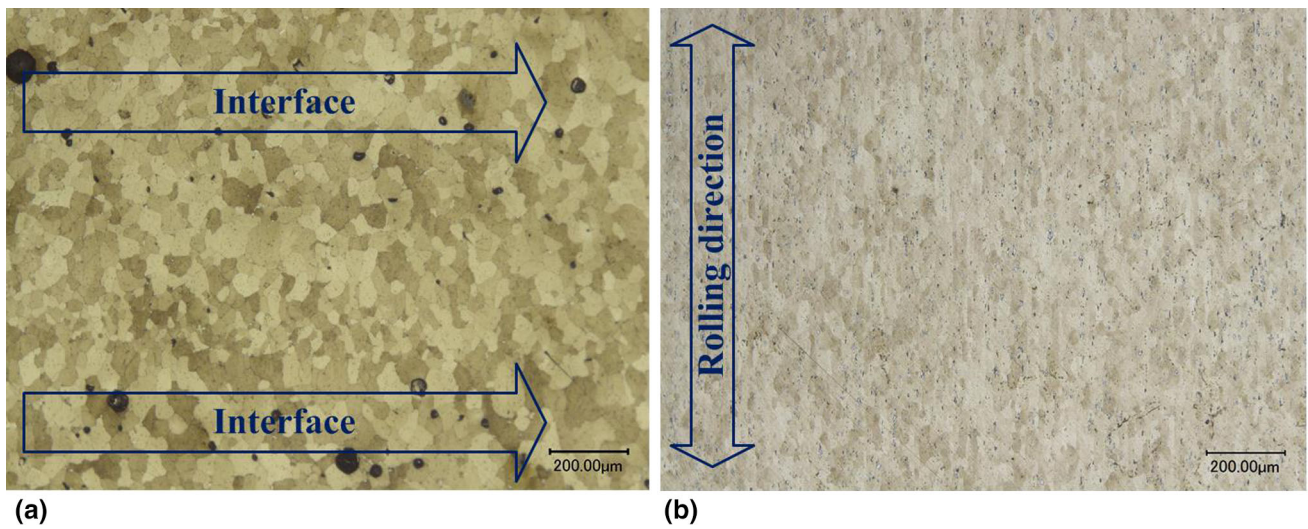


Fig. 13 Grains and porosities in (a) deposit + T6 2219-Al and (b) conventional casting + T6 2219-Al

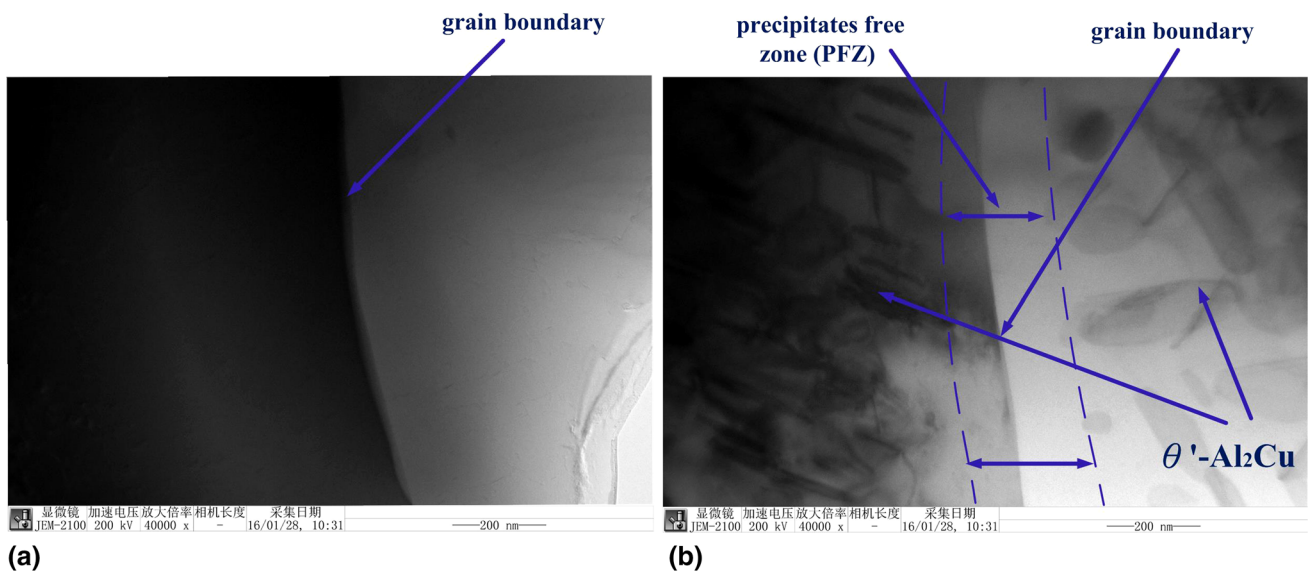


Fig. 14 TEM photographs of **a** grain boundaries in as-deposited 2219-Al and **b** precipitates free zone (PFZ) in deposit + T6 2219-Al

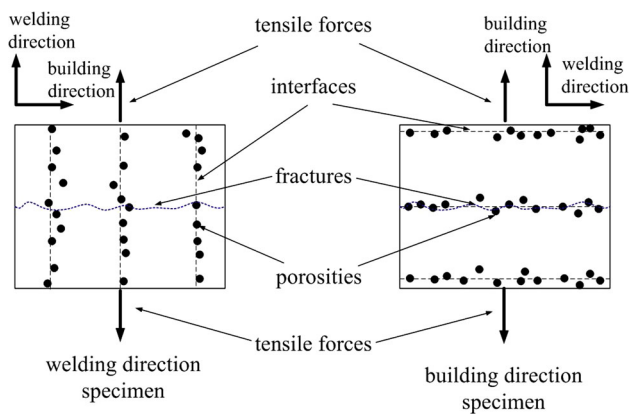


Fig. 15 Relationship between tensile forces and porosity distributions

grains and porosities. In deposit + T6 2219-Al, the sizes of the grains are inhomogeneous, which vary from 17 to 155 μm (Fig. 13a). Especially in the interface regions, many trivial grains and porosities make it an incongruous entity. While in conventional casting + T6 2219-Al, the spindly grains are very tiny and they are distributed along the rolling direction homogeneously (Fig. 13b). In tensile tests, the homogeneous microstructures contribute to a homogeneous dislocations' gliding behavior in conventional casting + T6 2219-Al. While in deposit + T6 2219-Al, the inhomogeneous microstructures lead to an inhomogeneous process. As a result, the deposit + T6 2219-Al has lower plasticity than casting + T6 2219-Al.

As for the weak property of the grain boundaries after heat treatment, they can be ascribed to the PFZs (precipitate-free zones). In as-deposited 2219-Al, both inner-grain regions and grain boundaries have no θ' - Al_2Cu phases (Fig. 14a). After heat treatment, many θ' - Al_2Cu phases precipitate from the α -Al matrix. The θ' - Al_2Cu phases strengthen the material, but the

distributions of θ' -Al₂Cu phases are not uniform when it comes to grain scale. In the inner region of the grains, the θ' phases are uniformly distributed. However, in the regions close to the grain boundaries, the θ' phases are vacant (Fig. 14b). Thus, there are precipitate-free zones (PFZs) near the grain boundaries. Because the value of σ_{ps} is much lower in PFZs, they become the weak points of the grain. Consequently, cracks are likely to propagate along the grain boundaries in tensile tests (Fig. 10d).

4.2 Mechanism of Anisotropic Strength

Anisotropies have been found in many kinds of materials, but the incentives are different. For example, in TC4, the columnar grains dominate. According to Hall–Petch (Ref 19), σ_{gbs} can be expressed as follows:

$$\sigma_{gbs} = bd^{-1/2} \quad (\text{Eq 5})$$

where b is a coefficient and d is the diameter of the grains. Since the columnar grains are strip shaped, the values of σ_{gbs} are different for building and welding directions. Thus, the anisotropy can be ascribed to the asymmetric morphologies of the grains in TC4.

However, the aforementioned mechanism does not fit well for 2219-Al. In 2219-Al, most of the grains are equiaxed structures (Fig. 13a and (Ref 11)). The diameters of the grains in the building and welding directions are identical. Thus, Eq 4 fails to explain the current phenomenon. Additionally, σ_{base} , σ_{ss} and σ_{ps} are non-directional, and therefore, there must be some other causes for 2219-Al.

As mentioned before, the belt-like distributing porosities need to be focused upon. Generally speaking, the damage of porosities to the tensile properties is due to the decrease in loading areas. Since porosities are more likely to occur at interfaces, the relationship between tensile force directions and porosities distribution directions should be carefully analyzed. As shown in Fig. 15, a more credible cause for anisotropy can be deduced.

In the welding direction specimen, the tensile force direction and porosity-distributing direction are parallel, and thus, the loading-area decreasing effect is very limited. In the building direction specimen, however, the tensile force direction and porosity-distributing direction are vertical. The decrease in the loading areas is more significant. So, a formula is developed and it takes into consideration the porosity-distributing feature. Consequently, the final value of deposit + T6 2219-Al (σ_{final}) should be expressed as follows:

$$\sigma_{final} = k\sigma_{deposit+T6} \quad (\text{Eq 6})$$

$$\sigma_{final} = k(\sigma_{base} + \sigma_{gbs} + \sigma_{ss} + \sigma_{ps}) \quad (\text{Eq 7})$$

where k ($k \leq 1$) is the loading-area decreasing coefficient. In reality, k increases with the decrease in porosities. When no porosity occurs at the interface, k is equal to 1. As mentioned before, the loading-area decreasing effect is more noticeable in the building direction. Thus, k is larger in the welding direction.

$$k^{weldingdirection} > k^{buildingdirection} \quad (\text{Eq 8})$$

Additionally, σ_{base} , σ_{gbs} , σ_{ss} and σ_{ps} are identical in two directions. According to Eq 6, 7 and 8, the σ_{final} is larger in the welding direction.

$$\sigma_{final}^{weldingdirection} > \sigma_{final}^{buildingdirection} \quad (\text{Eq 9})$$

5. Conclusions

1. The current homogenized solution + aging technique is an appropriate heat treatment for GTA-additive manufactured 2219-Al.
2. The hardness of deposit + T6 2219-Al is homogeneous in both part scale and layer scale.
3. The average ultimate strength and elongation of deposit + T6 2219-Al are 391 ± 28 Mpa and 8.3%. Compared to the properties of as-deposited 2219-Al, the ultimate strength has been improved by 65.0% at the expense of a 17% decrease in elongation.
4. In deposit + T6 2219-Al, most of the eutectic structures are dissolved. The porosities rather than the eutectic structures are the initiations of cracks. And the PFZs take the place of eutectic structures to be the propagating paths of cracks.
5. A revised formula has been put forward to calculate the strength of deposit + T6 2219-Al. The mentioned formula takes into consideration the belt-like porosity-distributing feature and scientifically describes the anisotropic properties in the material.

References

1. J.Y. Bai, J.H. Wang, S.B. Lin, C.L. Yang, and C.L. Fan, Width Prediction of Deposited Aluminium Alloy Manufactured by Shaped Metal Deposition with Tig, *Trans. China Weld. Inst.*, 2015, **36**, p 87–90 (in Chinese)
2. B. Baufeld, O.V. Biest, and R. Gault, Additive Manufacturing of Ti-6Al-4 V Components by Shaped Deposition: Microstructure and Mechanical Properties, *Mater. Des.*, 2013, **31**, p 106–111
3. S. Yang, M. Han, and Q. Wang, Development of a Welding System for 3D Steel Rapid Prototyping Process, *China Weld.*, 2001, **1**, p 50–56
4. J. Xiong and G.J. Zhang, Adaptive Control of Deposited Height in GMA-Based Layer Additive Manufacturing, *J. Mater. Process Tech.*, 2014, **214**, p 962–968
5. S.T. Skiba, B. Baufeld, and O.V. Biest, Shaped Metal Deposition of 300 M Steel, *Proc. Inst. Mech. Eng. B J Eng.*, 2011, **225**, p 831–839
6. H.J. Wang and R. Kovacevic, Rapid Prototyping of 4043 Al-Alloy Parts by VP-GTAW, *J. Mater. Process Tech.*, 2004, **148**, p 93–102
7. B. Baufeld, O.V. Biest, and R. Gault, Additive Manufacturing of Ti-6Al-4 V Components by Shaped Metal Deposition: Microstructure and Mechanical Properties, *Mater. Des.*, 2010, **31**, p 106–111
8. D. Clark, M.R. Bache, and M.T. Whittaker, Shaped Metal Deposition of a Nickel Alloy for Aero Engine Applications, *J Mater Process Tech.*, 2008, **203**, p 439–448
9. J.H. Wang, *Research on Shaped Metal Deposition of 2219 Aluminum Alloy by AC-TIG Welding*, Harbin Institute of Technology, Harbin, 2015 (in Chinese)
10. J.Y. Bai, C.L. Yang, S.B. Lin, B.L. Dong, and C.L. Fan, Mechanical Properties of 2219-Al Components Produced by Additive Manufacturing with TIG, *Int. J. Adv. Manuf. Technol.*, 2016, **86**, p 479–485
11. J.Y. Bai, C.L. Fan, S.B. Lin, C.L. Yang, and B.L. Dong, *Effects of Thermal Cycles on Microstructure Evolution of 2219-Al During GTA-Additive Manufacturing*, *Int. J. Adv. Manuf. Technol.*, 2016, **87**, p 2615–2623
12. B. Erhard and G. Daniel, Microstructure of Additive Layer Manufactured Ti–6Al–4 V After Exceptional Post Heat Treatments, *Mater. Lett.*, 2015, **81**, p 84–87
13. B. Erhard, S. Achim, and L. Christoph, Morphology, Microstructure, and Hardness of Titanium (Ti-6Al-4 V) Blocks Deposited by Wire-Feed Additive Layer Manufacturing (ALM), *Mater. Sci. Eng., A*, 2012, **532**, p 295–307

14. Y. Aref, S. Nima, M.T. Scott, and W.S. Denver, Effects of Process Time Interval and Heat Treatment on the Mechanical and Microstructural Properties of Direct Laser Deposited 316L Stainless Steel, *Mater. Sci. Eng., A*, 2015, **644**, p 171–183
15. F.J. Xu, *Microstructure Control and Process Optimization of Inconel 625 Alloy Fabricated by Plasma Arc Rapid Prototyping*, Harbin Institute of Technology, Harbin, 2013 (in Chinese)
16. Z.T. Wang, *Heat Treatment of Wrought Aluminum Alloy*, Central South University Press, Chang Sha, 2011 (in Chinese)
17. S. Malarvizhi and V. Balasubramanian, Effect of Welding Processes on AA2219 Aluminum Alloy Joint Properties, *Trans. Nonferrous Met. Soc. China*, 2011, **21**, p 962–973
18. B. Cong, B.J. Qi, and X.G. Zhou, Influences of Ultrasonic Pulse Square-Wave Current Parameters on Microstructure and Mechanical Properties of 2219 Aluminum Alloy Weld Joints, *Acta Metall. Sin.*, 2009, **45**, p 1057–1062
19. J.W. Wyrzykowski and M.W. Grabski, The Hall-Petch Relation in Aluminum and its Dependence on the Grain Boundary Structure, *Philos. Mag. A*, 1986, **53**, p 505–520